Rapid Communications

Orbital-selective metal-insulator transition lifting the t_{2g} band hybridization in the Hund metal $Sr_3(Ru_{1-x}Mn_x)_2O_7$

M. Nakayama,[1] Takeshi Kondo,[1,*] K. Kuroda,[1] C. Bareille,[1] M. D. Watson,[2] S. Kunisada,[1] R. Noguchi,[1] T. K. Kim,[2] M. Hoesch,[2,3] Y. Yoshida,[4] and S. Shin[1]

[1]*ISSP, University of Tokyo, Kashiwa, Chiba 277-8581, Japan*

[2]*Diamond Light Source, Harwell Campus, Didcot OX11 0DE, United Kingdom*

[3]*DESY Photon Science, Deutsches Elektronen-Synchrotron, Notkestrasse 85, 22607 Hamburg, Germany*

[4]*National Institute of Advanced Industrial Science and Technology, Electronics and Photonics Research Institute, Tsukuba, Ibaraki 305-8568, Japan*

(Received 16 March 2018; revised manuscript received 8 June 2018; published 3 October 2018)

We reveal the orbital-selective metal-insulator transition in a 4*d* multiorbital system, $Sr_3(Ru_{1-x}Mn_x)_2O_7$ ($x = 0-0.2$), by means of angle-resolved photoemission spectroscopy. With a small substitution ($x = 0.05$) of Mn with localized 3*d* orbitals, the spectra for the $4d_{xy}$ band become incoherent with a large gap, while the $4d_{xz/yz}$ bands stay metallic with sharp quasiparticle peaks. Intriguingly, this lifts band hybridization among 4*d* orbitals, and causes a two- to one-dimensional crossover in the remaining Fermi surface. Significant nesting in the remaining Fermi surface is implied to induce the reported magnetic ordering, and yields the insulating bulk state at higher Mn substitution, where all bands are gapped and totally incoherent. The availability of orbital-selective tuning of the pseudogap by a small impurity will prompt further theoretical studies of Hund's metals, which were recognized only recently in condensed matter physics.

DOI: 10.1103/PhysRevB.98.161102

Perovskite ruthenium oxides of the Ruddlesden-Popper type, $Sr_{n+1}Ru_nO_{3n+1}$, provide an excellent platform to investigate the effects of electron correlations in 4*d* multiorbital systems. Since 4*d* orbitals are more extended than 3*d* orbitals, they should experience smaller on-site Coulomb interactions than the latter. However, extremely large mass enhancements are experimentally observed in these bands [1,2]. It has been recently recognized that the Hund's exchange coupling J effectively increases the electron correlation, and plays a significant role of mass enhancement in multiorbital systems [3–11]. The local density approximation plus dynamical mean-field theory (LDA+DMFT) calculations demonstrate that these "Hund's metals" exhibit a coherent-incoherent crossover in the single-particle spectral function at elevated temperatures [8,12]. This has been indeed confirmed by angle-resolved photoemission spectroscopy (ARPES) for both 3*d*- and 4*d*-orbital materials such as iron-based chalcogenides and Sr_2RuO_4, respectively [12–16].

A remarkable property predicted for Hund's metals is orbital selectivity in the correlation effects [3,5,6]. Theory predicts that an orbital-selective Mott insulating ground state could emerge in Hund's metals as the on-site Coulomb interaction U/t is increased [3,5,6,17–19]. A promising candidate for such an intriguing state is Ca-substituted Sr_2RuO_4, and the verification for it has been claimed by ARPES for $Ca_{1.8}Sr_{0.2}RuO_4$ [20]. However, other ARPES results for the same composition show quasiparticle sharp peaks, regardless of band, which casts some doubt on this conclusion [21].

The observation of an orbital-selective insulating state has been reported for iron-based chalcogenides: At high temperatures, only the $3d_{xy}$ band completely loses spectral weight while the other $d_{xz/yz}$ bands remain itinerant [13,14], as expected by calculations for Hund's metals [8,11,12]. The experimental realization of orbital-selective insulating state as the ground state in matter has been still lacking to date, and thus it is strongly desired in condensed matter physics.

A rather unique metal-to-insulator transition has been reported in $Sr_3(Ru_{1-x}Mn_x)_2O_7$ [22,23]. Significantly, only a few percent ($\geqslant 5\%$) of Mn substitution onto the Ru site causes a phase change, turning the correlated paramagnetic metal into an antiferromagnetic insulator. The carrier doping and structural distortion of RuO_6 by such a small Mn doping is negligible [23], thus the band filling and bandwidth control will not be the driving mechanism for the insulator transition. The remarkable sensitivity to light Mn doping suggests that a significant 3*d*-4*d* interplay is responsible for the phase transition [24], and an unexpected orbital-selective nature might lie hidden in the intriguing materials.

In this Rapid Communication, we use angle-resolved photoemission spectroscopy, which is best suited to investigate the band-dependent properties of materials, and find an orbital-selective insulator transition upon cooling for crystals with a small concentration of Mn ($x = 0.05$, or 5%) in $Sr_3(Ru_{1-x}Mn_x)_2O_7$. Interestingly, this causes a two- to one-dimensional change in the topology of the Fermi surface due to the lifting of the contribution of the d_{xy} orbital to the t_{2g} band hybridization. Our results indicate that the incorporation of a small number of impurity sites with localized 3*d* orbitals can selectively tune the orbital-dependent interaction in 4*d* orbitals, leading to a drastic reconstruction of the multibands and the consequent emergence of antiferromagnetic ordering.

Single crystals of $Sr_3(Ru_{1-x}Mn_x)_2O_7$ (or RuMn327) were grown by the conventional floating-zone technique. The

*kondo1215@issp.u-tokyo.ac.jp

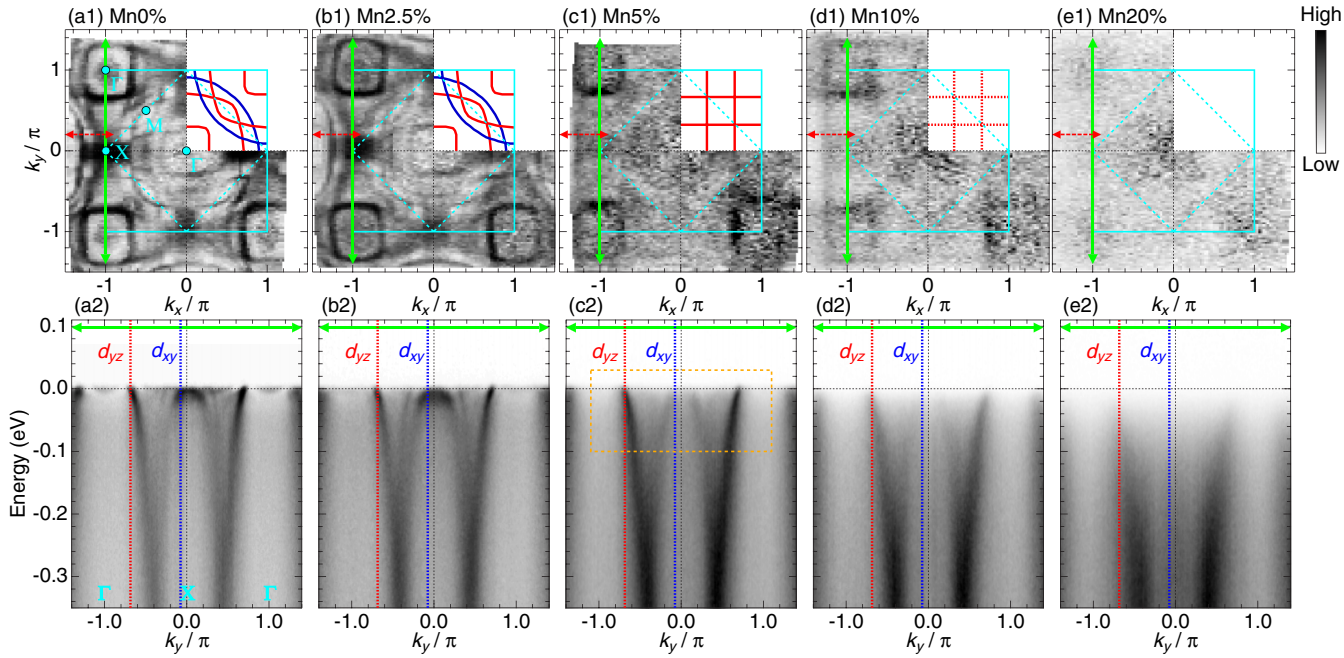

FIG. 1. The evolution of the electronic structure with Mn substitution in $Sr_3(Ru_{1-x}Mn_x)_2O_7$. (a1)–(e1) Fermi surface mapping from $x = 0$ (Mn 0%) to $x = 0.2$ (Mn 20%). Fermi surfaces for d_{xy} and $d_{xz/yz}$ bands are schematically illustrated with blue and red curves in each panel; here, the bilayer splitting is not represented for simplicity. The cyan dotted lines indicate the Brillouin zone reduced by rotation of RuO_6 octahedra in the crystal. (a2)–(e2) ARPES band dispersion measured along Γ-X-Γ [green arrows in (a1)–(e1)]. The blue and red dotted lines indicate k_F for d_{xy} and d_{yz} bands, respectively.

surface measured by ARPES is the (001) plane. To get a clean surface, a typical cleavage method was used: A top post glued on the crystal surface is hit *in situ* to break the crystal. The ARPES experiments were performed at beamline I05 at the Diamond Light Source, UK, with a Scienta R4000 analyzer. The photon energy used was 70 eV. The overall energy resolution was set to ∼12 meV in our experiments.

The variation of the electronic structure with Mn substitution in RuMn327 is examined in Fig. 1. Figures 1(a1)–1(e1) plot the ARPES intensities at the Fermi level (E_F) measured at a low temperature (10 K). In these compounds, the crystallographic RuO_6 octahedral rotations by ∼7° generate a reduced Brillouin zone (cyan dotted line), which folds back bands about it [23,25]. The pristine samples (Mn 0%) exhibit multiple Fermi-surface (FS) sheets derived from d_{xy} and $d_{xz/yz}$ orbitals [Fig. 1(a1)] (see the schematically drawn red and blue curves, respectively). These show almost no change with a slight substitution of Mn by 2.5% for the Ru site [Fig. 1(b1)]. A drastic variation, however, occurs by further substitution: First, the intensity of the d_{xy} band disappears in Mn 5% [Fig. 1(c1)], then those from the $d_{xz/yz}$ bands also become almost invisible in Mn 10% [Fig. 1(d1)]. Eventually, all the intensities, regardless of band, are completely lost at E_F in Mn 20% [Fig. 1(e1)], indicative of the insulating state in the bulk. These remarkable variations are also observed in ARPES band maps of Figs. 1(a2)–1(e2), which are obtained along a high-symmetry line Γ-X-Γ [green arrows in Figs. 1(a1)–1(e1)]: An abrupt suppression of spectral weight at E_F occurs only for the d_{xy} band in Mn 5% [Fig. 1(c2)]. It is followed by a relatively more gradual decrease of spectral intensities near E_F for the d_{yz} band at a higher Mn concentration [Figs. 1(d2) and 1(e2)].

To examine the spectral variation in more detail, we extract energy distribution curves (EDCs) at k_F from Figs. 1(a2)–1(e2) (red and blue dashed lines) in Figs. 2(a) and 2(b) for d_{yz} and d_{xy} bands, respectively. With increasing Mn concentration, the spectral weight of the quasiparticle peaks diminishes, and eventually becomes incoherent with a gap opening on both bands. We find, however, a clear difference between the two bands in Mn 5%: While a quasiparticle peak remains in the d_{yz} band [dotted red circle in Fig. 2(a)], it disappears and a gap opens in the d_{xy} band. This is visualized in Supplemental Figs. S1(a3) and S1(a4) by symmetrizing the EDCs about E_F to eliminate the effect of the Fermi cutoff [26]. We note that this result is insensitive to the selection of the k_F point since the spectral gaps are detected widely around the k_F points [see Supplemental Figs. S1(a2) and S1(a3) [26]]. The orbital selectivity is also confirmed in Fig. 2(c), which compares momentum distribution curves (MDCs) at E_F extracted along the red arrows in Figs. 1(a1)–1(e1). The peak for the d_{xy} band (blue arrows) vanishes across 5% of Mn substitution. This contrasts to the behavior of the d_{xz} band that the MDC peak (red arrows) is clearly observed in Mn 5% and it more gradually diminishes with increasing Mn concentration. Our data thus indicate that the Mn impurity with localized $3d$ orbitals preferentially enhances a correlation in the $4d_{xy}$ band, yielding an orbital-selective transition in Mn 5%.

We find distinct temperature evolutions of spectra between the $d_{xz/yz}$ and d_{xy} bands in Mn 5%. Figure 3(a1) plots EDCs at k_F of the d_{yz} band measured at elevated temperatures from 5 K (bottom) up to 60 K (top). The location of k_F is indicated in Figs. 3(d1) and 3(d2) with the red dotted lines. The spectral shape is almost identical for all the temperatures. This is further confirmed in Fig. 3(a2), in which all the EDCs are

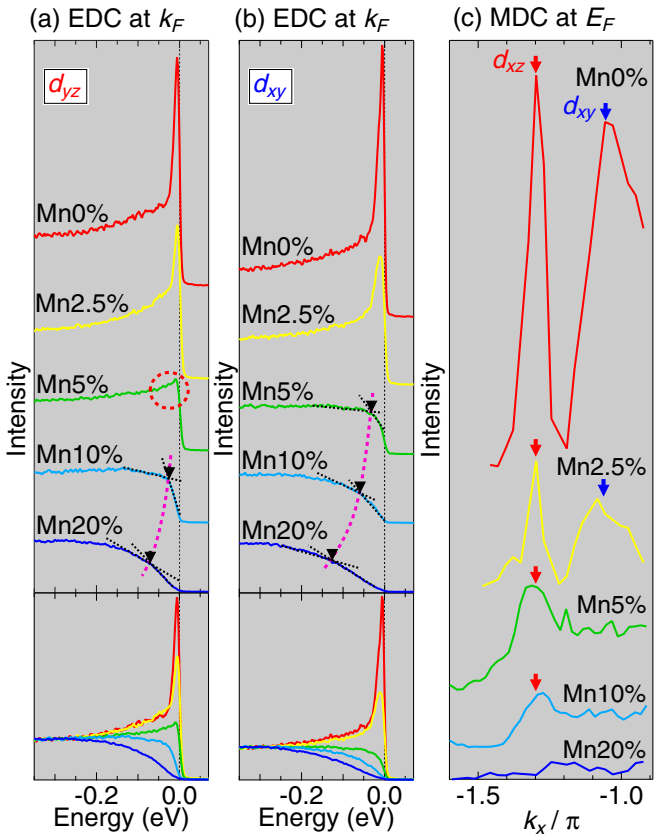

FIG. 2. Orbital selectivity revealed in ARPES spectra. (a), (b) EDCs at k_F of the d_{yz} and d_{xy} band, respectively, for various Mn concentrations, plotted with (top) and without (bottom) an offset. The black triangles and purple dotted curves indicate an energy gap and its increase with Mn concentration. The dotted red circle in (a) indicates a quasiparticle peak for Mn 5%, which is absent in the corresponding EDC of (b). (c) MDCs extracted along red arrows in Figs. 1(a1)–1(e1). The red and blue arrows indicate peaks for the d_{xz} and d_{xy} bands, respectively.

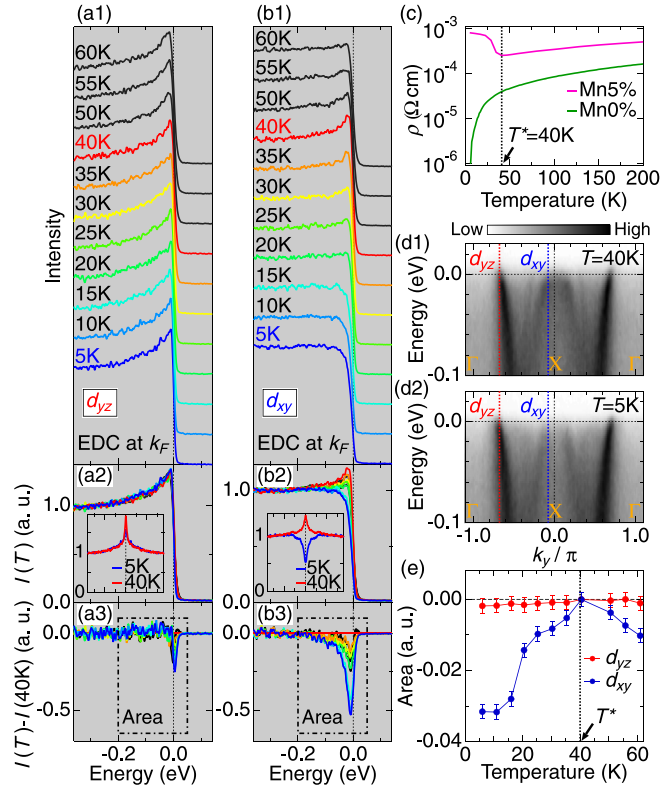

FIG. 3. The temperature evolution of the electronic structure in Mn 5%. (a1), (a2) Temperature evolution of EDCs at k_F for the d_{yz} band [red dotted lines in (d1) and (d2)] plotted with and without an offset, respectively. (a3) EDC at each temperature is subtracted by that at the transition temperature ($T^* = 40$ K). (b1)–(b3) Similar data to those in (a1)–(a3), but obtained at k_F for the d_{xy} band [blue dotted lines in (d1) and (d2)]. (c) Temperature dependence of resistivity $\rho(T)$ for pristine (Mn 0%) and Mn 5% samples. The metal-insulator-like transition is marked by an arrow at $T^* = 40$ K. (d1), (d2) ARPES band dispersion along Γ-X-Γ measured at $T = 40$ K and $T = 5$ K, respectively [dotted rectangular region in Fig. 1(c2)]. (e) The area of the difference spectra in (a3) and (b3) integrated over an energy window marked by a dotted box.

overlapped without an offset. These curves subtracted by the EDC at a high temperature of 40 K show only a small variation coming from thermal broadening [Fig. 3(a3)]. Therefore, the spectral intensities integrated within the energy window marked by a dotted box are estimated to be almost zero over the measured temperature range [red circles in Fig. 3(e)].

A rather unique temperature dependence in the spectra, which is clearly distinct from that for the d_{yz} band, is obtained in the d_{xy} band [Fig. 3(b1)]: A quasiparticle peak at k_F [blue dotted lines in Figs. 3(d1) and 3(d2)] emerges on heating, and grows up to 40 K, which is the temperature identified with a metal-insulator-like transition (T^*) estimated from the resistivity behavior shown in Fig. 3(c). This variation can be more clearly identified by plotting these spectra without a offset [Fig. 3(b3)]. We confirm that the energy gap closes above T^* [also see symmetrized EDCs in Supplemental Fig. S1(b3) [26]]. With a further increase of temperature, the quasiparticle peaks are strongly suppressed, while the gap remains closed, mostly due to a crossover into a bad metallic state induced by a temperature above 60 K [8]; this suppression is negligible in the d_{yz} band, indicating that the Mn elements effectively induce an orbital-selective scattering of electrons [27]. The spectral evolution for the d_{xy} band is summarized in Fig. 3(e) (blues circles), which plots the spectral weight lost due to a gap opening and/or a peak suppression close to E_F estimated as an area of difference spectra from that at the transition temperature ($T^* = 40$ K) within the energy window marked by a dotted box in Fig. 3(b3). The obtained behavior apparently differs from that for the d_{yz} band (red circles).

In perovskite ruthenium oxides, two-dimensional (2D)-like d_{xy} and one-dimensional (1D)-like $d_{xz/yz}$ orbitals are hybridized to form Fermi surfaces which are all 2D with round topology [28–30]. In particular, the band hybridization should most significantly occur along the $(0, 0)$-(π, π) direction, where all the bands get closest to each other in momentum space [31,32]. In Mn 5%, the d_{xy} band is gapped and incoherent at low temperatures, thus it should be excluded from contributing to the band hybridization. We could capture a relevant variation in FSs across the transition temperature ($T^* = 40$ K). Figures 4(a1) and 4(b1) exhibit high-quality

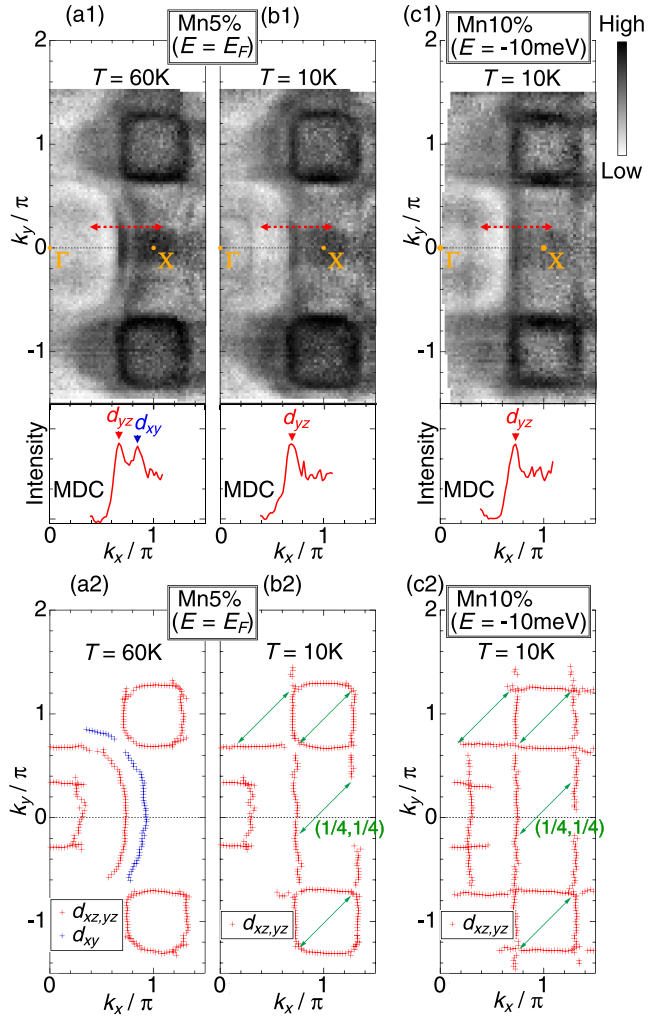

FIG. 4. The reconstruction of the Fermi surface across T^*. (a1), (b1) Top: ARPES intensity map at E_F for Mn 5% obtained above and below T^* ($T = 60$ and 10 K, respectively). Bottom: MDCs extracted along red arrows on the top panels. (a2), (b2) Fermi-surface plots corresponding to (a1) and (a2), respectively, determined from spectral peak positions. (c1) Top: ARPES intensity map slightly below E_F ($E = -10$ meV) for Mn 10%, obtained at $T = 10$ K. Bottom: MDC extracted along a red arrow on the top panel. (c2) Energy contours at $E = -10$ meV determined from MDC peaks in (c1). In (b2) and (c2), q vectors of (1/4, 1/4) corresponding to antiferromagnetic ordering are plotted.

FS maps measured in a fine step of angle above and below T^* ($T = 60$ and 10 K), respectively. A typical MDC along a red arrow on each FS map is extracted in the bottom of Figs. 4(a1) and 4(b1), which demonstrates that the peak only for the d_{xy} band (blue arrow) vanishes below T^*. In Figs. 4(a2) and 4(b2), the FS sheets are determined from spectral peaks: red and blue crosses for the $d_{xz/yz}$ and d_{xy} bands, respectively. The FS for the d_{xy} band (blue crosses), clearly seen at high temperatures, disappears below T^* over the entire Brillouin zone. As a consequence, we found that the round shape of the FS for the $d_{xz/yz}$ bands [see Fig. 4(a2)] becomes straight [see Fig. 4(b2)] since there is no longer a possibility of hybridizing with the d_{xy} band. The remaining straight 1D-like FSs are expected for bands derived only from $d_{xz/yz}$ orbitals.

Significantly, the 1D-like FSs left at low temperatures in Mn 5% have large segments connected by a single q vector of (1/4, 1/4), which is the same as the periodicity of antiferromagnetic ordering [33]. The good nesting, however, seems not to open an energy gap in the $d_{xz/yz}$ bands, in agreement with the resistivity behavior, which shows only a slight increase on cooling below T^* [see Fig. 3(b)]. However, upon further Mn substitution, gaps eventually open up in these 1D $d_{xz/yz}$ bands which have almost perfect nesting established near E_F [Fig. 4(c2) for Mn 10%]. In Mn 20%, the spectral weight near E_F becomes almost zero, thus the nesting is less important (see Supplemental Fig. S2 [26]). This is compatible to the disappearance of (1/4, 1/4) antiferromagnetic ordering in this composition. In a typical Peierls-like transition, caused by FS nesting, one would expect a reconstruction of the band dispersions and Fermi surface, but the observation of quasiparticle peaks would be expected to persist. Such behavior has been detected in $Ca_3Ru_2O_7$ by ARPES [34], consistent with its metallic resistivity down to the lowest temperatures. However our observations here are anomalous, in that the near-perfect FS nesting occurs in an incoherent, insulating state.

The orbital-selective transition we found at low temperatures in RuMn327 clearly differs from the temperature-induced crossover to an orbital-selective incoherent state reported for iron-based chalcogenides [13,14], which occurs at high temperatures, as expected by DMFT calculations for Hund's metals [8]. An alternative mechanism will be required for the observed transition in RuMn327. X-ray absorption spectroscopy has identified that Mn impurities have a 3+ valence (four $3d$ electrons), rather than 4+ (three $3d$ electrons), and the extra electron occupies the in-plane $3d_{x^2-y^2}$ orbital [24]. Importantly, the RuO_6 in these compounds is slightly rotated by $\sim 7^\circ$ [23], thus the nodal lines and lobes of the $d_{x^2-y^2}$ and d_{xy} orbitals are not directly pointing to the oxygen. This situation could allow mixing between the two orbitals, hence a significant hybridization between these bands [35]. The localized $3d_{x^2-y^2}$ orbital of Mn impurities [24], therefore, may induce a strong correlation preferentially in the in-plane $4d_{xy}$ band, and eventually yield the orbital-selective transition. Further theoretical input, however, would be required to confirm this scenario.

In conclusion, we present the orbital-selective incoherent ground state in a $4d$ multiorbital system, $Sr_3Ru_{2-x}Mn_xO_7$, by using ARPES. For $x = 0.05$, we find that only the d_{xy} band becomes gapped and incoherent at low temperatures, while $d_{xz/yz}$ bands remain metallic with quasiparticle peaks. Our results thus indicate that the localized $3d$ orbital of Mn impurities preferentially induces an incoherent property in the $4d_{xy}$ band and yields the orbital-selective insulating state. Interestingly, this lifts the t_{2g} band hybridization and brings the perfectly nested FS, which eventually triggers a bulk insulator at higher Mn concentrations. The orbital selectivity of the pseudogap state controlled by a small impurity should be an ingriguing aspect of Hund's metals with correlated multiorbitals, which requires further theoretical research on the mechanism.

We thank Takashi Koretsune, Ryotaro Arita, and Kozo Okazaki for fruitful discussions. This work was supported by the JSPS KAKENHI (17J09173, 16H06013, 16K13829,

16H00979, 16H02209, 25220707, 17K14319, 18H01165), and by the Photon and Quantum Basic Research Coordinated Development Program from MEXT. We thank Diamond Light Source for access to beamline I05 (Proposals No. SI16161 and No. SI15095) that contributed to the results presented here.

[1] A. P. Mackenzie and Y. Maeno, Rev. Mod. Phys. **75**, 657 (2003).
[2] C. Bergemann, A. P. Mackenzie, S. R. Julian, D. Forsythe, and E. Ohmichi, Adv. Phys. **52**, 639 (2003).
[3] A. Georges, L. de' Medici, and J. Mravlje, Annu. Rev. Condens. Matter Phys. **4**, 137 (2013).
[4] K. Haule and G. Kotliar, New J. Phys. **11**, 025021 (2009).
[5] L. de' Medici, S. R. Hassan, M. Capone, and X. Dai, Phys. Rev. Lett. **102**, 126401 (2009).
[6] L. de' Medici, Phys. Rev. B **83**, 205112 (2011).
[7] L. de' Medici, J. Mravlje, and A. Georges, Phys. Rev. Lett. **107**, 256401 (2011).
[8] J. Mravlje, M. Aichhorn, T. Miyake, K. Haule, G. Kotliar, and A. Georges, Phys. Rev. Lett. **106**, 096401 (2011).
[9] K. M. Stadler, Z. P. Yin, J. von Delft, G. Kotliar, and A. Weichselbaum, Phys. Rev. Lett. **115**, 136401 (2015).
[10] L. Fanfarillo and E. Bascones, Phys. Rev. B **92**, 075136 (2015).
[11] X. Deng, K. Haule, and G. Kotliar, Phys. Rev. Lett. **116**, 256401 (2016).
[12] T. Kondo, M. Ochi, M. Nakayama, H. Taniguchi, S. Akebi, K. Kuroda, M. Arita, S. Sakai, H. Namatame, M. Taniguchi, Y. Maeno, R. Arita, and S. Shin, Phys. Rev. Lett. **117**, 247001 (2016).
[13] M. Yi, D. H. Lu, R. Yu, S. C. Riggs, J. H. Chu, B. Lv, Z. K. Liu, M. Lu, Y. T. Cui, M. Hashimoto, S. K. Mo, Z. Hussain, C. W. Chu, I. R. Fisher, Q. Si, and Z. X. Shen, Phys. Rev. Lett. **110**, 067003 (2013).
[14] M. Yi, Z. K. Liu, Y. Zhang, R. Yu, J. X. Zhu, J. J. Lee, R. G. Moore, F. T. Schmitt, W. Li, S. C. Riggs, J. H. Chu, B. Lv, J. Hu, M. Hashimoto, S. K. Mo, Z. Hussain, Z. Q. Mao, C. W. Chu, I. R. Fisher, Q. Si, Z. X. Shen, and D. H. Lu, Nat. Commun. **6**, 7777 (2015).
[15] S. C. Wang, H. B. Yang, A. K. P. Sekharan, H. Ding, J. R. Engelbrecht, X. Dai, Z. Wang, A. Kaminski, T. Valla, T. Kidd, A. V. Fedorov, and P. D. Johnson, Phys. Rev. Lett. **92**, 137002 (2004).
[16] T. E. Kidd, T. Valla, A. V. Fedorov, P. D. Johnson, R. J. Cava, and M. K. Haas, Phys. Rev. Lett. **94**, 107003 (2005).
[17] A. Koga, N. Kawakami, T. M. Rice, and M. Sigrist, Phys. Rev. Lett. **92**, 216402 (2004).
[18] A. Liebsch, Phys. Rev. Lett. **95**, 116402 (2005).
[19] L. de' Medici, A. Georges, and S. Biermann, Phys. Rev. B **72**, 205124 (2005).
[20] M. Neupane, P. Richard, Z. H. Pan, Y. M. Xu, R. Jin, D. Mandrus, X. Dai, Z. Fang, Z. Wang, and H. Ding, Phys. Rev. Lett. **103**, 097001 (2009).
[21] A. Shimoyamada, K. Ishizaka, S. Tsuda, S. Nakatsuji, Y. Maeno, and S. Shin, Phys. Rev. Lett. **102**, 086401 (2009).
[22] R. Mathieu, A. Asamitsu, Y. Kaneko, J. P. He, X. Z. Yu, R. Kumai, Y. Onose, N. Takeshita, T. Arima, H. Takagi, and Y. Tokura, Phys. Rev. B **72**, 092404 (2005).
[23] B. Hu, G. T. McCandless, V. O. Garlea, S. Stadler, Y. Xiong, J. Y. Chan, E. W. Plummer, and R. Jin, Phys. Rev. B **84**, 174411 (2011).
[24] M. A. Hossain, Z. Hu, M. W. Haverkort, T. Burnus, C. F. Chang, S. Klein, J. D. Denlinger, H. J. Lin, C. T. Chen, R. Mathieu, Y. Kaneko, Y. Tokura, S. Satow, Y. Yoshida, H. Takagi, A. Tanaka, I. S. Elfimov, G. A. Sawatzky, L. H. Tjeng, and A. Damascelli, Phys. Rev. Lett. **101**, 016404 (2008).
[25] A. Tamai, M. P. Allan, J. F. Mercure, W. Meevasana, R. Dunkel, D. H. Lu, R. S. Perry, A. P. Mackenzie, D. J. Singh, Z. X. Shen, and F. Baumberger, Phys. Rev. Lett. **101**, 026407 (2008).
[26] See Supplemental Material at http://link.aps.org/supplemental/10.1103/PhysRevB.98.161102 for the symmetrization analysis of ARPES spectra and the detailed comparison of ARPES intensity maps for different Mn dopings.
[27] A. Herbig, R. Heid, and J. Schmalian, Phys. Rev. B **94**, 094512 (2016).
[28] A. Damascelli, D. H. Lu, K. M. Shen, N. P. Armitage, F. Ronning, D. L. Feng, C. Kim, Z. X. Shen, T. Kimura, Y. Tokura, Z. Q. Mao, and Y. Maeno, Phys. Rev. Lett. **85**, 5194 (2000).
[29] H. Iwasawa, Y. Yoshida, I. Hase, S. Koikegami, H. Hayashi, J. Jiang, K. Shimada, H. Namatame, M. Taniguchi, and Y. Aiura, Phys. Rev. Lett. **105**, 226406 (2010).
[30] H. Iwasawa, Y. Yoshida, I. Hase, K. Shimada, H. Namatame, M. Taniguchi, and Y. Aiura, Phys. Rev. Lett. **109**, 066404 (2012).
[31] M. W. Haverkort, I. S. Elfimov, L. H. Tjeng, G. A. Sawatzky, and A. Damascelli, Phys. Rev. Lett. **101**, 026406 (2008).
[32] C. N. Veenstra, Z. H. Zhu, M. Raichle, B. M. Ludbrook, A. Nicolaou, B. Slomski, G. Landolt, S. Kittaka, Y. Maeno, J. H. Dil, I. S. Elfimov, M. W. Haverkort, and A. Damascelli, Phys. Rev. Lett. **112**, 127002 (2014).
[33] D. Mesa, F. Ye, S. Chi, J. A. Fernandez-Baca, W. Tian, B. Hu, R. Jin, E. W. Plummer, and J. Zhang, Phys. Rev. B **85**, 180410 (2012).
[34] F. Baumberger, N. J. C. Ingle, N. Kikugawa, M. A. Hossain, W. Meevasana, R. S. Perry, K. M. Shen, D. H. Lu, A. Damascelli, A. Rost, A. P. Mackenzie, Z. Hussain, and Z. X. Shen, Phys. Rev. Lett. **96**, 107601 (2006).
[35] E. Ko, B. J. Kim, C. Kim, and H. J. Choi, Phys. Rev. Lett. **98**, 226401 (2007).